Journal of Alloys and Compounds 797 (2019) 589–594

Contents lists available at ScienceDirect

Journal of Alloys and Compounds

journal homepage: http://www.elsevier.com/locate/jalcom

Microstructures and properties of hybrid copper matrix composites reinforced by TiB whiskers and TiB_2 particles

Shuhua Liang**, Weizhen Li, Yihui Jiang*, Fei Cao, Gezhi Dong, Peng Xiao

Shaanxi Province Key Laboratory for Electrical Materials and Infiltration Technology, Xi'an University of Technology, Xi'an, Shaanxi 710048, China

ARTICLE INFO

Article history:
Received 15 March 2019
Received in revised form
8 May 2019
Accepted 11 May 2019
Available online 15 May 2019

Keywords:
Copper matrix composite
Hybrid reinforcement
Particle
Whisker

ABSTRACT

Hybrid copper matrix composites reinforced by TiB whiskers and TiB_2 particles were fabricated by in situ mixing casting in combination with rolling and annealing. During turbulent mixing and copper mold casting processes, the in situ reactions carried out completely, and the macrosegregation of reinforcements in the composites was overcome efficiently. By controlling the rolling and annealing parameters, unfavorable casting defects, including "chain-type" reinforcement clusters and shrinkage porosities that formed during the end stage of solidification, were eliminated. Accordingly, the uniform distribution of hybrid reinforcements in the as-annealed composites provided good comprehensive performance. Compared to the 2.6 wt%TiB_{2p}/Cu composite, the (1.0 wt%TiB_{2p}-0.9 wt%TiB_w)/Cu hybrid composite exhibited both higher strength (492 MPa) and higher electrical conductivity (85.5% International Annealed Copper Standard). Therefore, the hybrid effect in the copper matrix composites can be explained by the fact that a better strengthening effect was achieved by adding less hybrid reinforcement, which helped maintain the electrical conductivity at a relatively high level.

1. Introduction

Copper matrix composites (CMCs) have attracted much attention for their potential applications as electrical materials owing to their high strengths and high electrical conductivities [1–5]. However, there is generally an inverse relationship between these two properties. Therefore, selecting appropriate reinforcement materials is particularly important for fabricating CMCs with desirable comprehensive properties. TiB_2 is well known for its high hardness (2200 VHN [6]), high elastic modulus (565 GPa [6]) and high thermal stability. In particular, TiB_2 exhibits excellent low electrical resistance ($9 \times 10^{-8}\,\Omega\,m$ [6]), which is similar to the electrical resistances of some metals. These features make TiB_2 a highly preferred reinforcement in CMCs.

Among the various in situ fabrication methods for TiB_2/Cu composites, casting is of particular interest because it is inexpensive and in situ reactions occur rapidly and efficiently in molten copper [7]. Several advanced casting technologies have been developed to achieve uniform distributions of TiB_2 particles in copper matrices, such as turbulent in situ mixing casting [8], double-beam melt casting [3] and rotating magnetic field-aided casting [9]. However, the amount of TiB_2 added in as-cast CMCs is often at a relatively low level ($\leq$5 wt%) [3,8,9] because substantial aggregations of TiB_2 can still occur at high concentrations even when such advanced technologies are used. For this reason, further strengthening of as-cast TiB_2/Cu composites cannot be achieved by increasing the reinforcement concentration.

Recently, hybrid metal matrix composites [10–12] have received increasing attention because the performance of composites can be further improved by a cooperative strengthening effect of different reinforcements rather than by increasing the additive concentration. Typically, the advantages of hybrid reinforcements composed of whiskers and particles have been clearly shown in many metal matrix composites, such as (SiC_w-SiC_p)/Al composites [10], and (TiB_w-TiC_p)/Ti composites [11], where the subscripts w and p represent whiskers and particles, respectively. However, whether the hybrid effect is efficient in CMCs is less clear. According to thermodynamic and kinetic analyses, TiB_w and TiB_{2p} can be simultaneously formed in Cu-Ti-B ternary liquid alloys [13]. TiB_w is a promising reinforcement for fabricating CMCs due to its low electrical resistance ($3.4 \times 10^{-7}\,\Omega\,m$) and high elastic modulus (450 GPa) [6]. Based on the above considerations, the aim of this work is to use an in situ mixing casting process to fabricate hybrid

* Corresponding author.
** Corresponding author.
E-mail addresses: liangsh@xaut.edu.cn (S. Liang), jiangyihui@xaut.edu.cn (Y. Jiang).

https://doi.org/10.1016/j.jallcom.2019.05.129
0925-8388/

CMCs reinforced with TiB_w and TiB_{2p}. The hybrid effect is thus discussed on the basis of microstructural evolutions and composite properties.

2. Experiment

Using pure Cu (purity 99.9%), Ti (purity 99.99%) and B (purity 99.9%), two master alloys of Cu-Ti and Cu-B were first prepared by vacuum induction melting under a protective argon atmosphere. To fabricate uniform composites, a special vacuum casting device was designed, as shown in the schematic diagram in Fig. 1. The two master alloys had the same weight and were separately heated to 1473 K in a vacuum medium-frequency induction melting furnace. After a 2 min isothermal dwell, the two molten master alloys were simultaneously poured into a mixer at the same flow rate to form TiB_w and TiB_{2p} precipitates via chemical reactions between Ti and B. A "Z-type" channel in the mixer was designed for rigorous mixing of the two master alloys. The mixed liquid alloy was then cast into a copper mold to form hybrid composites with different nominal compositions, as shown in Table 1. The as-cast billets were rolled at 1173 K to a 30% reduction in thickness and then further rolled at room temperature to a total of 90% reduction in thickness. Finally, the as-rolled specimens were annealed at 533 K for 1 h. Comparative specimens of the TiB_{2p}/Cu composites and pure Cu were also prepared by the same procedure.

The phase compositions of the in situ fabricated composites were determined by X-ray diffraction (XRD, XRD-7000S, Shimadzu) using Cu-Kα radiation. The microstructures of the specimens were characterized using scanning electron microscopy (SEM, JSE-6700F, JEOL) and transmission electron microscopy (TEM, JEM-3010, JEOL). The chemical compositions of as-cast composites were analyzed by inductively coupled plasma atomic emission spectroscopy (ICP-AES, Agilent 725, Agilent). The average compositions of as-cast composite III was determined to be Cu-2.45 at.%Ti-3.49 at.%B, which is very close to the nominal composition. Tensile tests were performed with an electronic universal testing machine (HT2402, Hung Ta Instrument Co., Ltd) at room temperature with a displacement rate of 0.5 mm/min. Electrical conductivity, expressed in International Annealed Copper Standard (IACS), was measured by an eddy-current instrument. Specimens for SEM observation were prepared by mechanical grinding and electrolytic polishing with a solution containing 70% phosphoric acid in ethanol. TEM specimens were thinned in a precision ion polishing system (Model 691, Gatan). Plate tensile test specimens were machined from the fabricated composites. Each tensile specimen had a gauge length of 20.0 mm, width of 6.0 mm and thickness of 1.5 mm and was fixed to the two clamping fixtures of the tensile testing machine. The surfaces of the tensile specimens were polished to enable the observation of crack morphologies and propagations.

Table 1
Nominal compositions and reinforcement concentration of different as-cast composites.

Sample	Nominal composition			Theoretical concentration
	Ti, at.%	B, at.%	Cu, at.%	
Composite I	1.2	1.8	Balance	0.7 wt%TiB_{2p} + 0.6 wt%TiB_w
Composite II	1.8	2.7	Balance	1.0 wt%TiB_{2p} + 0.9 wt%TiB_w
Composite III	2.4	3.6	Balance	1.4 wt%TiB_{2p} + 1.2 wt%TiB_w
Composite IV	2.3	4.6	Balance	2.6 wt%TiB_{2p}
Pure Cu	–	–	100	0

3. Results

3.1. Microstructural evolution

Fig. 2 shows the XRD patterns of the as-cast composite III, where the relatively weak diffraction peaks were identified as the reflections of TiB and TiB_2 phases. Bright-field TEM images of the as-cast composite III are also shown in Fig. 3. With selected area electron diffraction (SAED), two kinds of reinforcements with different morphologies were identified as TiB whisker and TiB_2 hexagonal particles. The results of the XRD and TEM analyses confirm that the in situ reactions of Ti + 2B → TiB_2 and Ti + B → TiB occurred during the mixing and casting procedures. Furthermore, the lattice parameter of the Cu matrix can be calculated from the XRD patterns by using the method described in Ref. [14]. Applying the angle reflections of (111), (200) and (220) in Fig. 2, a measured value of 0.36185 nm is obtained for the lattice parameter; this result is close to the lattice parameter of as-cast pure copper

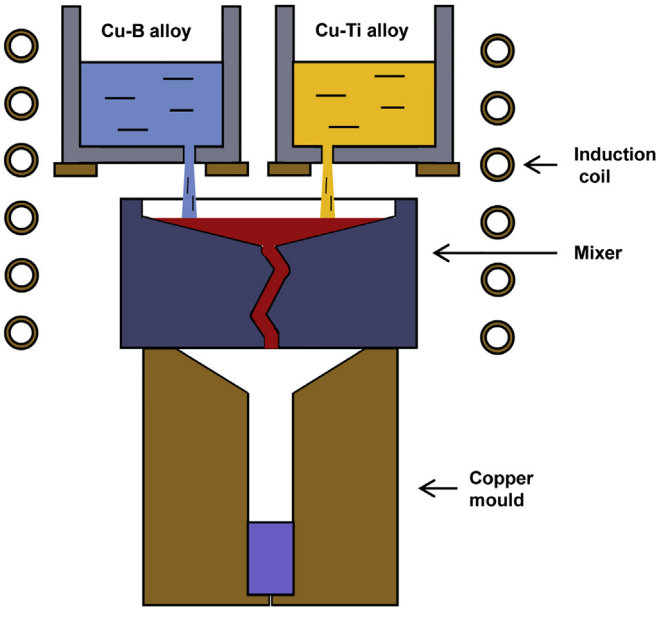

Fig. 1. Schematic diagram of a casting device for the fabrication of (TiB_w-TiB_{2p})/Cu composites.

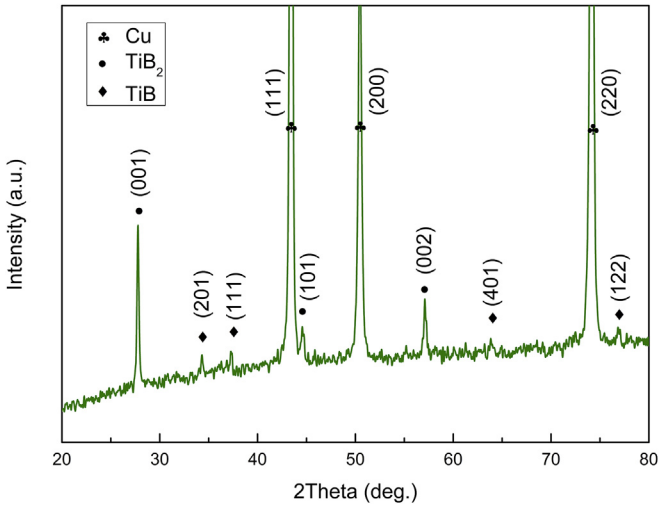

Fig. 2. XRD patterns of the as-cast (1.4 wt%TiB_{2p}-1.2 wt%TiB_w)/Cu hybrid composite.

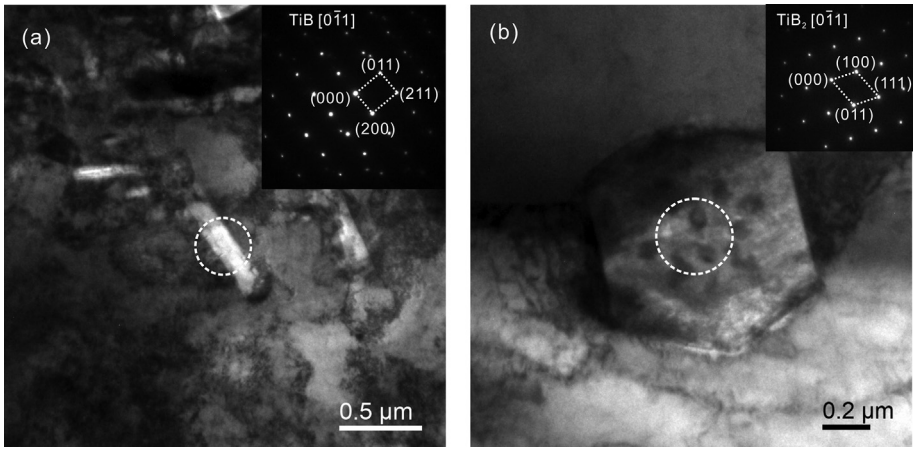

Fig. 3. Bright-field TEM images of the as-cast (1.4 wt%TiB_{2p}-1.2 wt%TiB_w)/Cu hybrid composite: (a) TiB whisker and (b) TiB_2 particle.

(0.36178 nm [15]), which indicates that the content of the solid solution elements in the copper matrix of the as-cast composite III is very low and that the in situ reactions are complete.

After precipitating from the mixed liquid, the distribution states of the reinforcements in the as-cast composites mainly depend on the solidification process. The overall microstructures of the as-cast billets were examined by transversely sectioning different parts of each billet; however, no significant difference was observed in the same billet. This finding suggests that the gravity-induced macrosegregation has been efficiently overcome as a result of the turbulent mixing and rapid solidification achieved by using the device shown in Fig. 1. Typical SEM images of the as-cast composite III and composite IV are shown in Fig. 4. Microsegregation of the in situ formed reinforcements occurred in both composites, which tended to manifest as a "chain-type" cluster. In addition, shrinkage porosity is often observed around the cluster, as shown in Fig. 4b. The reinforcement of composite IV (Fig. 4a) is mainly composed of TiB_2 particles with sizes of 0.1–0.5 μm. By comparison, the microstructure of composite III (Fig. 4b) contains several different features, such as forming a hybrid whisker and particle reinforcement, larger particle sizes (1–10 μm), and less microsegregation.

To eliminate the unfavorable casting defects of microsegregation and shrinkage porosity, rolling processes were applied to the composites. Using hot rolling with a 30% reduction in thickness, the shrinkage porosity in the as-cast composite III was removed, but most of the "chain-type" clusters were retained due to the insufficient deformation of hot rolling (see Fig. 5a). After severe cold-rolling and stress-relief annealing, Fig. 5b shows that the cluster chain was broadened in the as-annealed composite III. The results shown in Fig. 5 imply that the composites were homogenized and densified by the rolling and annealing processes. Furthermore, the relatively density, which is calculated by the ratio of measured Archimedes density relative to calculated theoretical density, was increased from 97.6% in as-cast composite III to 99.5% in as-annealed composite III. It confirms that the composites were densified by the post-processing treatments.

3.2. Composite properties

The stress-strain curves of the as-cast and as-annealed specimens are presented in Fig. 6. The corresponding ultimate tensile strengths and yield strengths are shown in Table 2. The mechanical properties of the composites are remarkably impacted by the reinforcement type, concentration, and processing state. First, the strengths of the hybrid composites increase as the reinforcement concentration increases while the total reinforcement amount is less than 2.6 wt%. Among the specimens under the same processing state, composite III exhibits the highest strength. For example, the as-cast composite III has a yield strength of 188 ± 16 MPa, which is 90% higher than that of pure Cu (99 ± 6 MPa). Second, Fig. 6 also shows that the strengths of the composites are dramatically enhanced by rolling and annealing due to the effects of work-hardening and elimination of casting defects. Third, the strengths of the hybrid composites are much higher than those of composites reinforced by a single type of particle. For example, the as-annealed hybrid composite III exhibits a yield strength of 520 ± 17 MPa, which is 19% higher than the as-annealed composite IV (438 ± 15 MPa) reinforced by the same reinforcement concentration.

The measured electrical conductivities of the as-cast and as-annealed composites are also gathered in Table 2. Obviously, the electrical conductivity monotonically decreases as the reinforcement concentration increases. By comparing the as-annealed composites to the as-cast composites, the electrical conductivity

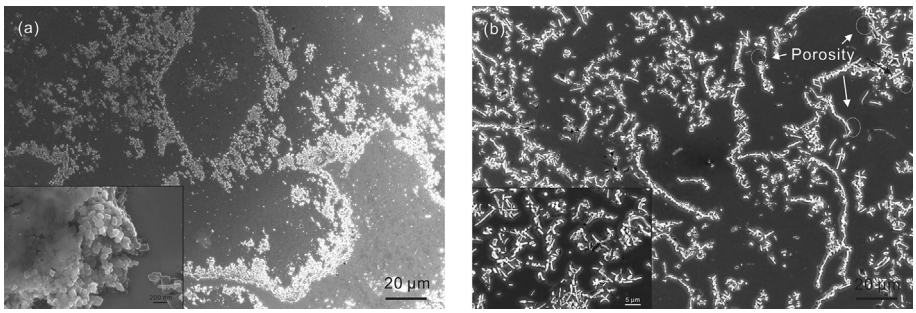

Fig. 4. SEM images of (a) the as-cast 2.6 wt%TiB_{2p}/Cu and (b) the as-cast (1.4 wt%TiB_{2p}-1.2 wt%TiB_w)/Cu composites.

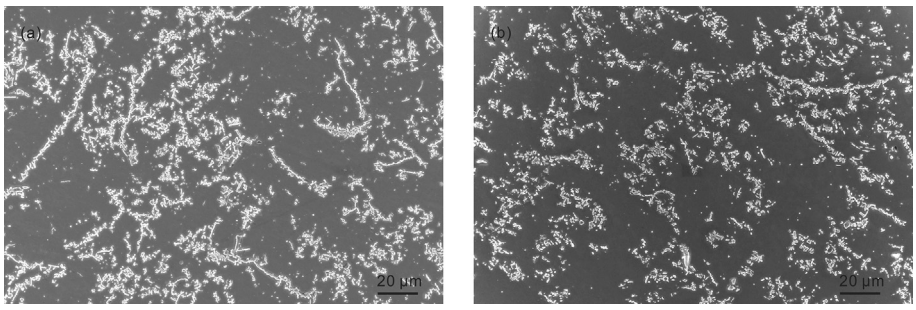

Fig. 5. SEM images of the (1.4 wt%TiB_{2p}-1.2 wt%TiB_w)/Cu hybrid composite after (a) hot rolling and (b) annealing.

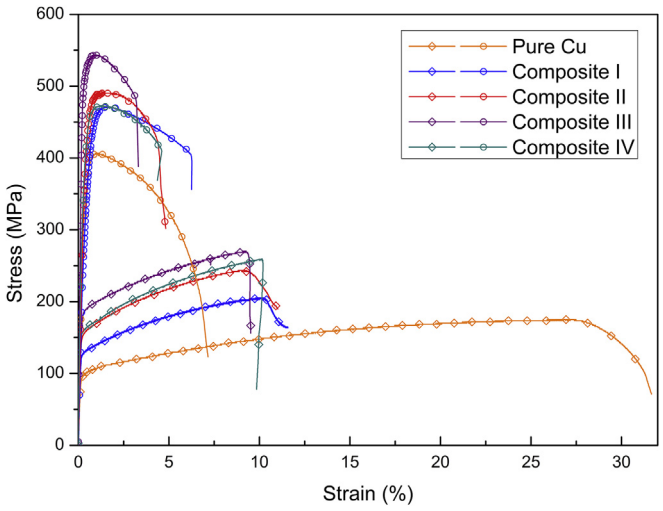

Fig. 6. Tensile stress-strain curves of the fabricated composites at different processing states: as-cast specimens (diamond symbol) and as-annealed specimens (circle symbol).

is remarkably improved by rolling and annealing because of the induced densification. Furthermore, by replacing a portion of TiB_{2p} with an equivalent weight of TiB_w, the electrical conductivity of composite III is slightly lower than that of composite IV.

4. Discussion

4.1. Formation mechanisms of the as-cast composite microstructures

According to the microstructural characteristics shown in Fig. 4a, the formation of clusters in the as-cast TiB_{2p}/Cu composite can be mainly attributed to two reasons. First, the heterogeneous nucleation of TiB_2 may occur after mixing the two master alloys. It has been reported that the {001} planes of TiB_2 can act as a nucleation substrate for itself [16]. The heterogeneous nucleation mechanism was often employed to describe the precipitation of TiB_2 particles in liquid alloys [13]. In Fig. 4a, the small particle sizes of TiB_2 (0.1–0.5 μm) implies that a high nucleation rate occurs during the formation of TiB_2, which is a key feature of heterogeneous nucleation. The smaller TiB_2 particles, in turn, tend to form large clusters for reducing interface energy [17] because of the poor wettability of TiB_2 particles by molten copper [9]. Second, the "chain-type" clusters may result from a phenomenon of particle pushing by a solid-liquid interface. During the solidification of metal matrix composites, ceramic particles interact with the solid-liquid interface [7]. For a certain system, the particle size and solidification velocity are critical parameters to determine whether the particle is pushed or engulfed by the solidification front [18]. In this case, the particle size should be replaced by its equivalent cluster size because of agglomeration. The cluster size induced by heterogeneous nucleation is too large to be engulfed inside grains even at a rapid cooling rate. Accordingly, the formation mechanism of the microstructures in the as-cast TiB_{2p}/Cu composites becomes apparent. The heterogeneous nucleation of the TiB_2 phase at the mixing stage causes the TiB_2 particles to agglomerate into large clusters, which were pushed by solidification front to form "chain-type" clusters during solidification.

Compared to the TiB_{2p}/Cu composite, the difference in the microstructures of the (TiB_{2p}-TiB_w)/Cu hybrid composite (Fig. 4b) can be mainly attributed to the variations in the nucleation mechanism. To fabricate hybrid composites, the chemical composition of mixed liquid alloy may not be suitable for the heterogeneous nucleation of the TiB_2 phase. The initial atomic ratio of Ti: B in the mixed liquid alloy is 2 : 3, as shown in Table 1. If a TiB_2 particle has precipitated, the atomic ratio of Ti: B in the surrounding liquid becomes 1 : 1, which is more appropriate for forming TiB nuclei rather than TiB_2 nuclei in the neighboring region around previously formed TiB_2 particles. As a result, the heterogeneous nucleation of the TiB_2

Table 2
Mechanical and electrical properties of different composites at as-cast and as-annealed states.

Processing state	Sample	Ultimate tensile strength (MPa)	Yield strength (MPa)	Electrical conductivity (%IACS)	M ($\times 10^6$ MPa^2 %IACS)
As-cast	Pure Cu	175 ± 10	99 ± 6	93.1 ± 3.9	2.9
	Composite I	205 ± 13	130 ± 11	87.9 ± 3.1	3.7
	Composite II	244 ± 13	157 ± 12	80.2 ± 4.8	4.8
	Composite III	270 ± 19	188 ± 16	62.2 ± 5.4	4.5
	Composite IV	259 ± 12	160 ± 11	70.7 ± 5.1	4.7
As-annealed	Pure Cu	407 ± 13	378 ± 11	98.9 ± 0.5	16.8
	Composite I	471 ± 18	437 ± 14	91.2 ± 1.7	20.2
	Composite II	492 ± 18	442 ± 15	85.5 ± 1.1	20.7
	Composite III	543 ± 20	520 ± 17	75.2 ± 1.3	22.2
	Composite IV	472 ± 19	438 ± 15	81.4 ± 1.4	18.1

phase is inhibited, and the nucleation rate is substantially reduced. This assertion can be confirmed by the large particle sizes and coexistence of whiskers and particles in Fig. 4b. Due to the lack of conditions for forming large clusters, the majority of reinforcements will be engulfed inside growing copper grains to form a more dispersive microstructure during solidification. However, the solidification velocity will slow during the end stage due to latent heat release and the weakened chilling effect of the copper mold. Therefore, the interaction between the solid-liquid interface and reinforcing particles may be changed from engulfment to pushing, and a few "chain-type" clusters may form during the end stage of solidification. This point can be confirmed by the overlapping of the shrinkage porosity with the clusters (see Fig. 4b) because the shrinkage porosity is formed in the areas of the cast ingot that solidify later than the surroundings. Thus, a scenario of microstructure formations in hybrid composites can be proposed. The hybrid reinforcements precipitate and distribute uniformly in the liquid alloy after mixing, and a transition from engulfment to pushing mechanisms occurs during the end stage of solidification, which results in a substantially uniform microstructure with a few "chain-type" clusters.

4.2. Relationships between the microstructure and mechanical properties

In this section, tensile fractography is employed to analyze the mechanical properties of the fabricated composites, as shown in Fig. 7. In Fig. 7a, the fracture surface of the as-cast composite III is composed of ductile dimples of various sizes, which indicate a ductile fracture mode. According to the microstructure shown in Fig. 4b, fine dimples may be formed in the region containing dispersed reinforcements due to the pinning effect of the reinforcements, whereas large dimples may be formed in regions where the reinforcement is insufficient. In addition, a reinforcement cluster can be clearly observed in the fracture surface of the as-cast composite (see Fig. 7b). Since the "chain-type" clusters are often accompanied by shrinkage porosities, they act as a preferential site for microcrack initiation during tensile testing. This assertion can be confirmed by the observation of the polished specimen surface after tensile testing (see Fig. 7c). It can thus be concluded that the strengths of the as-cast composites are indeed improved by the addition of reinforcements, but the strengthening effect is limited due to the casting defects, which result in relatively low strengths, as shown in Fig. 6.

Fig. 7d shows a tensile fractograph of the as-annealed composite III, wherein a large number of uniform fine ductile dimples can be observed. Since the majority of casting defects have been removed (see Fig. 5b), the uniformly distributed reinforcements have been fully utilized to obtain a higher strength. Fig. 7e shows that the hexagonal TiB_{2p} can be clearly observed at the bottom of the dimples, but the whisker phase exhibits different morphologies. When the TiB_w orientation is approximately transverse to the loading direction, a strengthening effect similar to TiB_{2p} occurred; this is indicated by the black arrow in Fig. 7e, wherein the whiskers can be observed at the bottom of the dimples. However, if the TiB_w orientation is approximately parallel to the loading direction, whisker debonding and pull-out occurred, and the pulled-out whiskers and residual holes can be observed in Fig. 7e. Furthermore, fractured TiB_w can also be observed during crack propagation (see Fig. 7f), which suggests that the load transferred from the matrix to the whisker during the tensile test. It is believed that both the whisker pull-out and the whisker fracture can contribute to the improved work of a fracture and, as a result, increase the strengths of the composites [19].

4.3. Hybrid effect of the whiskers and particles in CMCs

According to the classical theory (i.e., the Maxwell model [20]), the electrical conductivities of CMCs depend on the properties and concentration of the reinforcement. In composites III and IV, the total reinforcement concentrations are equal, but an equivalent substitution of 1.2 wt% TiB_{2p} by 1.2 wt% TiB_w was made in composite III. Therefore, the higher electrical resistance of TiB_w leads to the slightly lower electrical conductivity of composite III compared to that of composite IV. However, even though composites I and II are reinforced by both whiskers and particles, these composites exhibit much higher electrical conductivities than composite IV because of the low reinforcement concentration. This suggests that

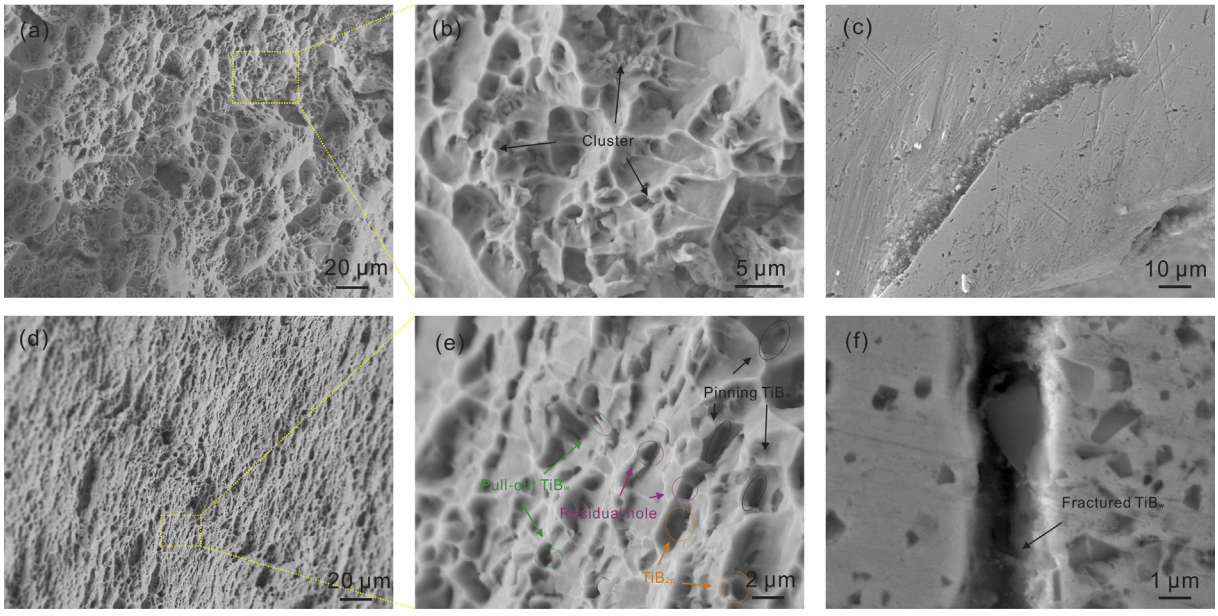

Fig. 7. Tensile fractographs and crack morphologies of (a–c) the as-cast and (d–f) the as-annealed (1.4 wt%TiB_{2p}-1.2 wt%TiB_w)/Cu hybrid composites.

the reinforcement concentration rather than the reinforcement type is the major factor for the reduction in electrical conductivity in hybrid composites.

For the case of mechanical properties, the hybrid effect can be illustrated as follows. The fractographic analysis indicates that the strengthening effect of the two reinforcements in CMCs is mainly due to the embedded hard phases in copper matrix and load transfer effect. Based on the Nardone and Prewo model [21], the load transfer effect of a whisker with a large aspect ratio is much greater than that of an equiaxed particle phase. Although the strengthening effect of a whisker is more effective than that of a particle, a pure whisker reinforcement also has its own deficiencies, such as its tendency to fracture (see Fig. 7f), which leads to substantial stress concentrations. Therefore, in hybrid composites, the effect of whiskers and particles will complement each other, which will result in higher mechanical properties. For the example shown in Fig. 6, the strength and elongation of composite II, which is reinforced by a lower content of hybrid phases, are even higher than those of composite IV, which are reinforced by a greater concentration of single TiB_2 phase.

Since both the strength and the electrical conductivity are important properties of electrical engineering materials, a combination index, M, was proposed to represent the comprehensive performance of copper materials. The M index can be expressed as follows [22]:

$$M = \sigma_b^2 \rho \quad (1)$$

where σ_b and ρ represent the ultimate tensile strength and the electrical conductivity, respectively. The values of the M index for different composites are gathered in Table 2. It can be seen that all the M values of the three hybrid composites are greater than that of composite IV. It is worth noting that, compared to composite IV, the higher M index of composite II is due to both a higher strength and a higher electrical conductivity. Therefore, the hybrid effect in the CMCs can be explained by the fact that a better strengthening effect is achieved by adding less hybrid reinforcement, which helps maintain the electrical conductivity at a relatively high level.

5. Conclusions

Using in situ mixing casting technology, the (TiB_{2p}-TiB_w)/Cu hybrid composites with completed reactions and inhibited macrosegregation were fabricated. Compared to the TiB_{2p}/Cu composite, the degrees of microsegregation in the as-cast hybrid composites are remarkably reduced due to the inhibited heterogeneous nucleation. After rolling and annealing, the hybrid composites exhibit densified and uniform microstructures. Due to the cooperative effects of the particles and whiskers, the hybrid composites exhibit both higher strength and higher electrical conductivity than the other composites. The hybrid effect in the CMCs can thus be explained by the fact that a better strengthening effect is achieved by adding less hybrid reinforcement, which helps maintain the electrical conductivity at a relatively high level.

Acknowledgments

This work was supported by the National Natural Science Foundation of China [grant numbers U1502274 and 51834009], the Key Research and Development Program of Shannxi [grant number 2017ZDXM-GY-028], and the Shaanxi Key Laboratory Program [grant numbers 13JS075 and 17JS081].

References

[1] S.C. Tjong, K.C. Lau, Tribological behaviour of SiC particle-reinforced copper matrix composites, Mater. Lett. 43 (2000) 274–280, https://doi.org/10.1016/S0167-577X(99)00273-6.
[2] G. Li, J. Sun, Q. Guo, R. Wang, Fabrication of the nanometer Al_2O_3/Cu composite by internal oxidation, J. Mater. Process. Technol. 170 (2005) 336–340, https://doi.org/10.1016/j.jmatprotec.2005.05.011.
[3] X. Guo, K. Shen, M. Wang, Relationship between microstructure, properties and reaction conditions for Cu–TiB_2 alloys prepared by in situ reaction, Acta Mater. 57 (2009) 4568–4579, https://doi.org/10.1016/j.actamat.2009.06.030.
[4] D.B. Xiong, M. Cao, Q. Guo, Z.Q. Tan, G.L. Fan, Z.Q. Li, D. Zhang, Graphene-and-copper artificial nacre fabricated by a preform impregnation process: bio-inspired strategy for strengthening-toughening of metal matrix composite, ACS Nano 9 (2015) 6934–6943, https://doi.org/10.1021/acsnano.5b01067.
[5] G.H.A. Bagheri, The effect of reinforcement percentages on properties of copper matrix composites reinforced with TiC particles, J. Alloys Compd. 676 (2016) 120–126, https://doi.org/10.1016/j.jallcom.2016.03.085.
[6] S. Madtha, C. Lee, K.S.R. Chandran, Physical and mechanical properties of nanostructured titanium boride (TiB) ceramic, J. Am. Ceram. Soc. 91 (2008) 1319–1321, https://doi.org/10.1111/j.1551-2916.2007.02246.x.
[7] M. Sobhani, H. Arabi, A. Mirhabibi, R.M.D. Brydson, Microstructural evolution of copper-titanium alloy during in-situ formation of TiB_2 particles, Trans. Nonferrous Metals Soc. China 23 (2013) 2994–3001, https://doi.org/10.1016/S1003-6326(13)62826-5.
[8] J.H. Kim, J.H. Yun, Y.H. Park, K.M. Cho, I.D. Choi, I.M. Park, Manufacturing of Cu-TiB_2 composites by turbulent in situ mixing process, Mater. Sci. Eng. A 449–451 (2007) 1018–1021, https://doi.org/10.1016/j.msea.2006.02.302.
[9] C. Zou, H. Kang, W. Wang, Z. Chen, R. Li, X. Gao, T. Li, T. Wang, Effect of La addition on the particle characteristics, mechanical and electrical properties of in situ Cu-TiB_2 composites, J. Alloys Compd. 687 (2016) 312–319, https://doi.org/10.1016/j.jallcom.2016.06.129.
[10] X.N. Zhang, L. Geng, G.S. Wang, Fabrication of Al-based hybrid composites reinforced with SiC whiskers and SiC nanoparticles by squeeze casting, J. Mater. Process. Technol. 176 (2006) 146–151, https://doi.org/10.1016/j.jmatprotec.2006.03.125.
[11] Y.L. Qin, L. Geng, D.R. Ni, Dry sliding wear behavior of titanium matrix composites hybrid-reinforced by in situ TiB_w and TiC_p, J. Compos. Mater. 46 (2011) 2637–2645, https://doi.org/10.1177/0021998311417645.
[12] S. Li, K. Kondohb, H. Imai, B. Chen, L. Jia, J. Umed, Y. Fu, Strengthening behavior of in situ-synthesized (TiC–TiB)/Ti composites by powder metallurgy and hot extrusion, Mater. Des. 95 (2016) 127–132, https://doi.org/10.1016/j.matdes.2016.01.092.
[13] Y. Jiang, D. Li, S. Liang, J. Zou, F. Liu, Phase selection of titanium boride in copper matrix composites during solidification, J. Mater. Sci. 52 (2017) 2957–2963, https://doi.org/10.1007/s10853-016-0592-2.
[14] J.B. Correia, H.A. Davies, C.M. Sellars, Strengthening in rapidly solidified age hardened Cu–Cr and Cu–Cr–Zr alloys, Acta Mater. 45 (1997) 177–190, https://doi.org/10.1016/S1359-6454(96)00142-5.
[15] Y. Jiang, D. Li, X. Zhang, J. Zou, P. Xiao, S. Liang, Effects of various strengthening methods on the properties of Cu–Ti–B alloys, Mater. Sci. Technol. 34 (2018) 340–346, https://doi.org/10.1080/02670836.2017.1390645.
[16] S. Hu, S. Li, H. Li, Y. Zhou, Large-scale growth of TiB_2 hexagonal platelets, J. Alloys Compd. 690 (2017) 930–935. https://doi.org/10.1016/j.jallcom.2016.08.208.
[17] A. Jha, C. Dometakis, The dispersion mechanism of TiB_2 ceramic phase in molten aluminum and its alloys, Mater. Des. (1997) 297–301, https://doi.org/10.1016/S0261-3069(97)00068-X.
[18] Y.M. Youssef, R.J. Dashwood, P.D. Lee, Effect of clustering on particle pushing and solidification behavior in TiB_2 reinforced aluminum PMMCs, Composites Part A 36 (2005) 747–763, https://doi.org/10.1016/j.compositesa.2004.10.027.
[19] J. Yin, D. Yao, H. Hu, Y. Xia, K. Zuo, Y.P. Zeng, Improved mechanical properties of Cu matrix composites reinforced with β-Si_3N_4 whiskers, Mater. Sci. Eng. A 607 (2014) 287–293, https://doi.org/10.1016/j.msea.2014.04.021.
[20] J.C. Maxwell, A Treatise on Electricity and Magnetism, third ed., Dover, New York, 1954, p. 435.
[21] V.C. Nardone, K.M. Prewo, On the strength of discontinuous silicon carbide reinforced aluminum composites, Scripta Metall. 20 (1986) 43–48, https://doi.org/10.1016/0036-9748(86)90210-3.
[22] L.M. Peng, X.M. Mao, K.D. Xu, W.J. Ding, Property and thermal stability of in situ composite Cu–Cr alloy contact cable, J. Mater. Process. Technol. 166 (2005) 193–198, https://doi.org/10.1016/j.jmatprotec.2004.08.013.